OPEN ACCESS
Journal of Innovative Optical Health Sciences
Vol. 14, No. 4 (2021) 2141005 (10 pages)

DOI: 10.1142/S1793545821410054

SERS devices with "hedgehog-like" nanosphere arrays for detection of trace pesticides

Yang Liu*,†, Xin Li*,†, Jie Cheng*,†, Na Zhou*,†, Lingqian Zhang*, Haiyang Mao*,†,‡,§ and Chengjun Huang*,†,¶

*Institute of Microelectronics of Chinese Academy of Sciences, Beijing 100029, P. R. China

†University of Chinese Academy of Sciences Beijing 100049, P. R. China

‡Wuxi Internet of Things Innovation Center Co. Ltd. Advanced Sensing Department, Wuxi 214001, P. R. China

§maohaiyang@ime.ac.cn

¶huangchengjun@ime.ac.cn

Received 26 April 2021
Accepted 19 May 2021
Published 23 June 2021

The development of surface-enhanced Raman scattering (SERS) devices for detection of trace pesticides has attracted more and more attention. In this work, a large-area self-assembly approach assisted with reactive ion etching (RIE) is proposed for preparing SERS devices consisting of Ag-covered "hedgehog-like" nanosphere arrays (Ag/HLNAs). Such a SERS device has an enhancement factor of 2.79×10^7, a limit of detection (LOD) up to 10^{-12} M for Rhodamine 6G (R6G) analytes, and a relative standard deviation (RSD) smaller than 10%, demonstrating high uniformity. Besides, for pesticide detections, the device achieves an LOD of 10^{-8} M for thiram molecules. It indicates that the proposed SERS device has a promising opportunity in detecting toxic organic pesticides.

Keywords: Surface-enhanced Raman scattering (SERS); self-assembly; Ag-covered "hedgehog-like" nanosphere arrays (Ag/HLNAs); pesticide detections.

1. Introduction

Crop loss caused by diseases, pests, and weeds accounts for 20–40% of overall agricultural production, pesticides with insecticidal and therapeutic abilities that are important in protecting agricultural production and reducing economic losses.[1]

Yang Liu and Xin Li contributed equally to this work.
§,¶Corresponding authors.

However, the use of pesticides is also accompanied by risks of environmental pollution and residues in food chains as there is an enrichment effect of trace pesticides, thus these risks cannot be ignored and have raised public concern.[2–4] From this point of view, trace detection of pesticides is of significance.

Since its discovery in 1974 by Fleischmann *et al.*, surface-enhanced Raman scattering (SERS) has been extensively researched.[5,6] It has a hopeful prospect as an analytical method for detecting trace organic chemicals even down to single-molecule level[7] with advantages of high sensitivity, fingerprint characteristics, and rapid detections.[8–10] To date, SERS has been commonly used in numerous fields including medical science,[11,12] bio-sensing,[13,14] and analytical chemistry.[15,16] For a SERS device, being sensitive and uniform is the key to obtain high-quality SERS spectra. In the early stage, a colloid chemistry strategy involving noble metal nanoparticles (NPs) was developed for SERS detections with high sensitivity. It is well accepted that the electromagnetic enhancement mechanism originating from localized surface plasmon resonances (LSPRs) in the noble metal NPs plays a dominant role in most SERS procedures.[17,18] However, the number and size of these noble metal nanoparticles constituting conglomerations are random, impeding the guarantee of consistent and reliable SERS signals.[19] To solve the problem, different periodic SERS substrates have been proposed. For instance, nanosphere arrays,[20] nanoantenna arrays,[21] nanopillar arrays,[22] nanoparticle or nanoshell arrays[23] were developed due to their good consistency and reliability. To fabricate highly sensitive SERS substrates with high uniformity, a wide range of approaches, including e-beam lithography (EBL),[24] femtosecond laser etching,[25] focused ion beam (FIB) technique[26] and metal-assisted chemical etching (MACE)[27] have been reported to prepare nanostructures with precise dimension and position control. Nevertheless, those fabrication processes are usually time-consuming and expensive. Simple and large-scale fabrication approaches for nanosubstrate with sufficient and uniform "hot spots" are still highly demanded for SERS-based trace analyte detections.

Herein, we demonstrate an effective reactive ion etching (RIE)-assisted self-assembly approach to fabricate a SERS device consisting of Ag-covered "hedgehog-like" nanosphere arrays (Ag/HLNAs), which provides abundant and uniformly distributed "hot spots" between the neighboring building blocks. The presented SERS device shows high sensitivity to Rhodamine 6G (R6G) probe molecules even when the concentration is lower to 10^{-12} M, and an ultrahigh EF of 2.79×10^7 is achieved. The relative standard deviation (RSD) is estimated smaller than 10%, demonstrating the device has excellent uniformity in SERS spectra. The limit of detection (LOD) of the device is tested to be 10^{-8} M for thiram. It is expected that the SERS device based on the novel Ag/HLNAs structures can obtain high sensitivity and good uniformity, thus providing a new approach for the detection of pesticides in foods.

2. Experimental

2.1. *Materials*

Aqueous suspensions of monodispersed spherical colloidal polystyrene (PS) nanospheres, with a coefficient of variation (CV) less than 3%, of 500 nm in diameter were purchased from Suzhou Knowledge & Benefit Sphere Tech. Co., Ltd. (Suzhou, China). Acetone and ethanol were purchased from Tianjin Fengchuan Chemical Reagent Technologies Co., Ltd. (Tianjin, China). Glass slides and silicone capillaries with a diameter of 0.5 mm were brought from Casmart (Beijing, China). N-type single-crystal silicon wafers with a thickness of $500 \pm 15\,\mu$m were purchased from Research Materials Microtech Co., Ltd (Suzhou, China). A target of pure silver (99.99%) was bought from GRIKIN Advanced Material Co., Ltd (Beijing, China). The SERS probe molecule R6G was purchased from J&K Scientific Co., Ltd (Beijing, China). Thiram was purchased from Sigma Aldrich Corporation (Shanghai, China). Deionized (DI) water (18.2 MΩ·cm^{-1}) used in experimental process was purified in an ultrafiltration system (Milli-Q, Millipore). All the solvents and chemicals were at least reagent grade and were used as received.

2.2. *Wafer-scale preparation of highly ordered 2D colloidal crystal monolayer*

The strategy to achieve a highly ordered colloidal monolayer without overlapping nanospheres has been described in detail in our previous work.[28]

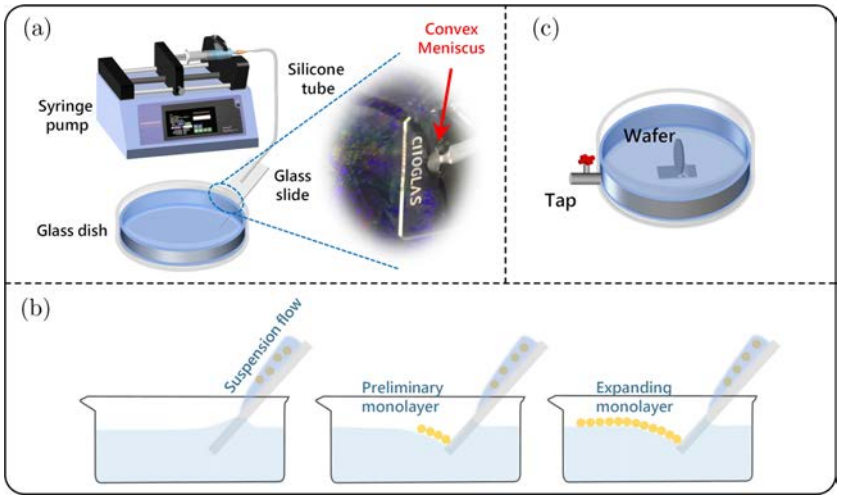

Fig. 1. Self-assembly near the three-phase boundary. (a) The graph of the adopted setup. (b) The diagram of the self-assembly process. (c) The holder used to keep the wafer vertical while transferring the colloidal monolayer from air/water interface to the target substrate by lowing the water level.

In brief, a glass slide, a silicone tube, and a syringe pump were adopted to form a confinement region for self-assembly near the three-phase boundary (air, water subphase, and glass slide) as shown in Fig. 1(a). When the colloidal suspension was injected into the air–water interface, a convex meniscus was formed as a result of drag force. With the confinement of the convex, the initial colloidal suspension, instead of spreading outward, directly self-assembled into a preliminary monolayer (Fig. 1(b)). Further, as soon as the subsequent PS nanospheres were released to the water surface, they were captured immediately by the preliminary monolayer and transformed into a stable monolayer. After the completion of the self-assembly process, the obtained PS colloidal monolayer was transferred to the target wafer by lowering the water level. To ultimately reduce the crystal defects, especially the overlapping nanospheres, a homemade holder was adopted to keep the wafer vertical as shown in Fig. 1(c). Finally, a nearly-perfect PS colloidal monolayer in wafer-scale was achieved with the average domain size up to centimeter scale.

2.3. *Preparation of "hedgehog-like" nanosphere arrays*

The process for preparing Ag-covered "hedgehog-like" nanosphere arrays (Ag/HLNAs) is depicted schematically in Fig. 2. Si substrates with PS nanosphere arrays packed closely in hexagon were put into the chamber of RIE apparatus (RIE-150, Beijing Zhongke Tailong Electronic Technology Co., Ltd., China) for O_2 plasma etching. During the process of plasma etching, the RF power was set at 50 W, the chamber pressure was 36 mTorr, and the flowing rate for O_2 was 200 sccm, respectively. Under these conditions, the treatment time of O_2 plasma lasted for 60 s. The aforementioned operation was performed twice and stopped for a period of time, in order to stabilize etching speed of the PS nanospheres by avoiding high temperature. Subsequently, HLNAs were obtained. Then, an Ag layer with a thickness of 10 nm was evaporated on rough surface of the HLNAs at a deposition rate of $0.3\,\text{Å}\cdot\text{s}^{-1}$ using DE400 EBEAM e-beam evaporation system (10 kV, 7×10^{-5} Pa). After the above procedures, Ag/HLNAs were acquired. For comparison, a flat Si substrate covered with Ag NPs was also fabricated simultaneously under the same evaporation conditions mentioned above.

2.4. *Electromagnetic field simulations*

The electromagnetic field distribution of the 2D structure and the HLNAs was simulated using finite difference time domain (FDTD) software. The diameter of the Ag NPs and PS nanospheres was set according to the average size measured by scanning electron microscope (SEM). A plane wave source (532 nm) with polarized light along the x-axis was used for light excitation from the top. To obtain relatively high precise field enhancement resolution, the grid size was set to $1\,\text{nm}\times1\,\text{nm}\times1\,\text{nm}$ with a

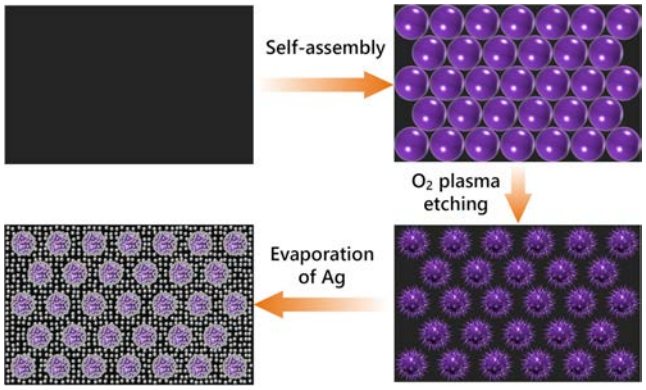

Fig. 2. Schematic fabrication procedures of Ag/HLNAs.

conformal variant 2 mesh refinement. Since the HLNAs were periodic in the lateral dimensions, only one unit cell was calculated with appropriate periodic boundary conditions adopted to the lateral side of the computational domain. The bottom and top parts of the domain were dealt with uniaxial perfectly matched layers to absorb the outgoing waves and thus mimic infinitely extended background. To properly compare the difference of the electromagnetic field distribution between the flat substrate and the HLNAs, an identical setting was applied to the flat substrate model.

2.5. *Characterization and SERS measurements*

SEM (Hitachi S-5500, Japan) with a primary electron energy of 3 kV was employed to characterize the morphologies of the as-prepared samples. SERS measurements were performed using a confocal Raman microscopy (inVia Reflex Raman microscope, Renishaw PLC, UK) equipped with a He-Ne laser of 532 nm, the excitation power was chosen as 0.05 mW and the integration time was set as 10 s. For the SERS measurements of R6G molecules, a series of 4 μL R6G solutions with a concentration gradient were dropped on surfaces of the samples and dried at room temperature. To obtain the spectra of thiram analytes, the samples were immersed into 0.5 mL thiram solutions with different concentrations for two h, taken out and then dried in air. For comparison, all the collected spectra were normalized by the laser power and integration time. After measurements, the data were processed by WiRE 3.2 software. Baseline correction was performed to suppress background noises.

3. Results and Discussion

3.1. *Characterization of Ag/HLNAs*

As shown in Fig. 3(a), highly ordered PS nanospheres arrays were easily formed at the three-phase boundary (air, water subphase, and glass slide) by the convex-meniscus-assisted self-assembly method. A partially enlarged image in Fig. 3(b) shows that the colloidal monolayer formed by self-assembly is virtually defect-free. Therefore, the high-quality stable 2D colloidal nanospheres arrays could further ensure high uniformity of Raman signals in subsequent SERS detections. Figure 3(e) schematically explains the formation mechanism of HLNAs. During the process of oxygen plasma etching of PS nanospheres, the chamber is filled with oxygen at a steady flow rate, and it maintains a low pressure under simultaneous pumping. Oxygen atoms are ionized under the action of a high-frequency electric field, and the oxygen plasma (reactive species)

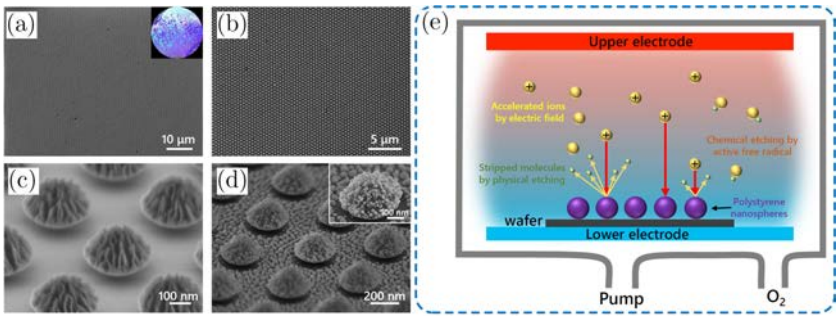

Fig. 3. SEM images of (a) closely-packed PS nanosphere arrays (top view). Inset shows a photograph of the colloidal monolayer on a 2-inch silicon wafer. (b) A zoom in view of the 2D PS single colloidal crystals. (c) HLNAs (angled view at 30° tilt). (d) Ag NPs-covered HLNAs (angled view at 30° tilt). Inset shows the corresponding nanostructures in high magnification. (e) Schematic diagram of etching mechanism and process of RIE apparatus.

containing oxygen ions and electrons, excited neutral particles, and photons, etc., is produced. The reactive species then attach to surfaces of the PS, break the C–C bonds and enhance the formation of low molecular-weight fragments. Subsequently, the further oxidization of the carbon and hydrogen produces volatile products including CO_2 and H_2O, which are released from the substrate and purged out *via* a vacuum system.[29] Hence, the PS size is decreased *in situ* with an increase in etching time. Meanwhile, the accelerated oxygen ions also physically strike surfaces of the PS spheres under a strong electric field. Therefore, due to the synergistic effect of both chemical and physical etching, the size of nanospheres is gradually reduced while nanospikes are formed on their surface, as shown in Fig. 3(c). The prepared Ag NPs-covered HLNAs for SERS measurements is presented in Fig. 3(d). In particular, lower evaporation rates lead to denser Ag NPs on surface of the HLNAs. Aggregated Ag NPs can form "hot spots" and greatly enhance the locally polarized electric field, resulting in significant Raman enhancement.

3.2. *Characterization of SERS capability*

R6G was used as a probe molecule to investigate SERS performance of SERS-active substrates. To evaluate the SERS effects, typical Raman spectra of 10^{-6} M R6G measured on the Ag-decorated flat Si, and HLNAs are shown in Fig. 4(a). The Ag/HLNAs present the strongest Raman signals of R6G molecules from these two types of substrate configurations. Figure 4(b) shows the Ag/HLNAs display the highest SERS intensities at different characteristic peaks. This phenomenon demonstrated the Ag NPs on the surfaces of HLNAs greatly enhance the LSPR coupling effect, leading to tremendous increase of Raman signals.

SERS measurements with different R6G concentrations were performed in order to assess the LOD of the Ag/HLNAs. The Raman spectra of Ag/HLNAs grafted with different R6G concentrations of 10^{-4} M, 10^{-6} M, 10^{-8} M, and 10^{-12} M are illustrated in Fig. 5(a). As the R6G concentration decays exponentially, the signal intensities at 613 cm^{-1}, 1362 cm^{-1}, 1511 cm^{-1}, and 1650 cm^{-1} decrease obviously. However, these characteristic peaks of R6G are still distinguishable at the low concentration of 10^{-12} M. The SERS spectra reveal the characteristic peaks of R6G at 613 cm^{-1} (C–C–C ring in-plane bending mode), 773 cm^{-1} (C–H out-of-plane bending mode), 1184 cm^{-1} (C−H in-plane bending mode), 1312 cm^{-1} (C–O stretching vibration mode), and 1362 cm^{-1}, 1511 cm^{-1}, and 1650 cm^{-1} (aromatic C–C stretching mode), respectively.[30] Figure 5(b) further illustrates the relationship between the R6G concentration and SERS spectral intensity at 613 cm^{-1}, 1362 cm^{-1}, 1511 cm^{-1}, and 1650 cm^{-1}. It indicates that SERS intensity increases rapidly with a large slope when the concentration of R6G is higher than 10^{-8} M. Meanwhile, there is an excellent linear response ranging at concentrations of 10^{-4}–10^{-8} M. The coefficient of determination

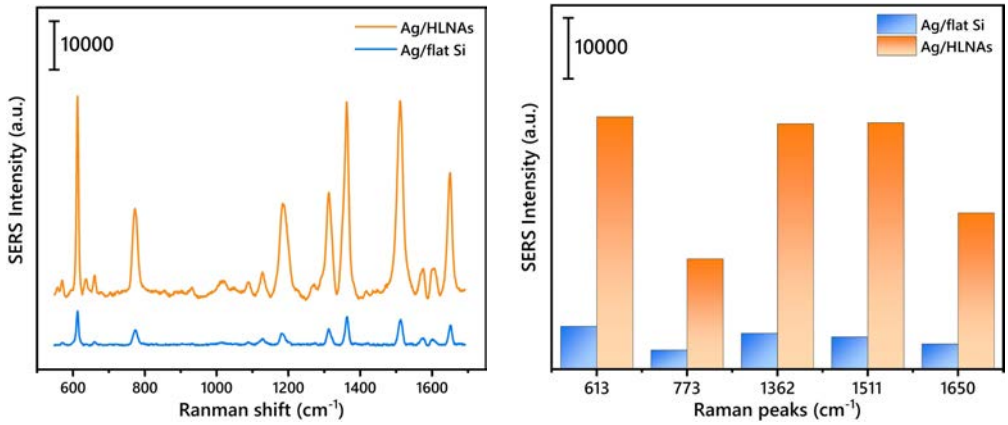

(a) (b)

Fig. 4. (a) Raman spectra of 10^{-6} M R6G measured on Ag/flat Si and Ag/HLNAs, respectively. (b) SERS intensities of these two substrates at 613 cm^{-1}, 773 cm^{-1}, 1362 cm^{-1}, 1511 cm^{-1}, and 1650 cm^{-1} in (a).

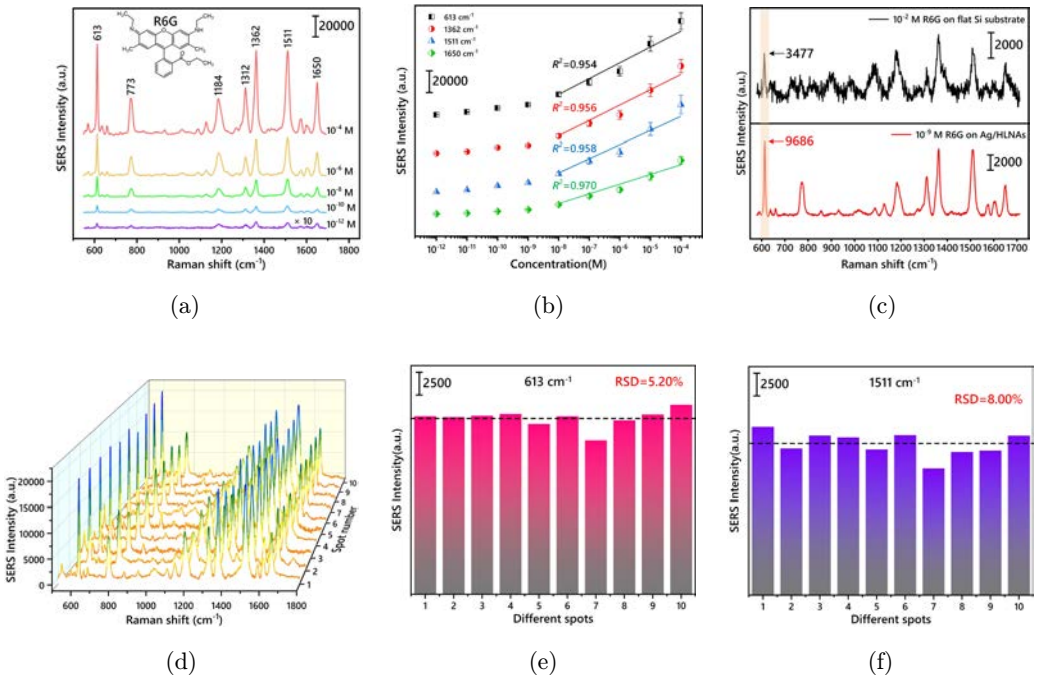

Fig. 5. (a) Raman spectra of different concentrations of R6G adsorbed on Ag/HLNAs. Inset shows the molecular structure of R6G. (b) SERS intensity-logarithmic plot of R6G at different concentrations of 10^{-4} M to 10^{-12} M from four characteristic peaks in (a). (c) SERS spectra of 10^{-2} M and 10^{-9} M R6G detected on flat Si substrate and Ag/HLNAs, respectively. (d) Raman spectra of 10^{-8} M R6G obtained from the Ag/HLNAs at 10 random positions. SERS intensities of characteristic peaks at (e) 613 cm^{-1} and (f) 1511 cm^{-1} collected from the spectra in (d).

(R^2) at 613 cm^{-1}, 1362 cm^{-1}, 1511 cm^{-1}, and 1650 cm^{-1} was calculated as 0.954, 0.956, 0.958, and 0.970, respectively.

To investigate the enhancement ability of the Ag/HLNAs demonstrably, the enhancement factors (EFs) of these typical Raman peaks were calculated by the following equation[31]:

$$\mathrm{EF} = \frac{I_{\mathrm{SERS}}}{I_{\mathrm{Raman}}} \times \frac{N_{\mathrm{Raman}}}{N_{\mathrm{SERS}}},$$

where I_{SERS} and I_{Raman} represent signal intensities obtained on the SERS substrate and reference

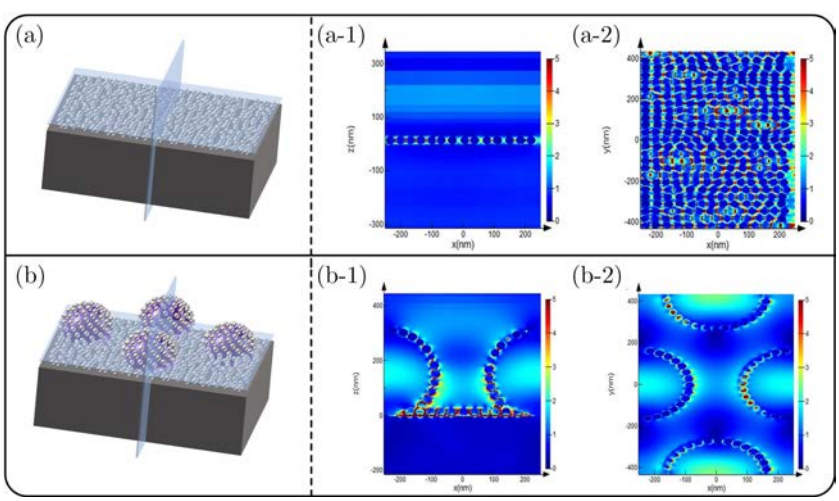

Fig. 6. The results of the FDTD simulation. (a, b) The simplified physical model of the planar structure and the Ag/HLNAs. (a-1, a-2) Vertical and parallel section views of the local electric field distribution in (a). (b-1, b-2) Vertical and parallel section views of the local electric field distribution in (b).

substrate at the same characteristic peaks, respectively. N_{SERS} and N_{Raman} are the number of excited probe molecules (R6G) in the SERS substrate and reference substrate under the same volume. Figure 5(c) depicts the reference spectrum of 10^{-2} M R6G obtained on flat Si substrate (black curve) and SERS spectrum obtained from 10^{-9} M R6G on Ag/HLNAs (red curve). After calculation, the maximum EF value of R6G triggered by Ag/HLNAs is 2.79×10^{7} at 613 cm^{-1}. In our SERS devices, the O_2 plasma treated PS nanospheres provided the curved and rough surfaces, which supplied a large area for decoration of Ag NPs. Compared with Ag/flat Si, the Ag/HLNAs provide more "hot spots" for SERS activities within the same excitation light area. In addition, the "hot spots" between Ag NPs located on surface of the flat Si contribute partly to the SERS signal improvement.

As an efficient SERS substrate, the uniformity needs to be verified. To evaluate the reproducibility of the Ag/HLNAs, SERS spectra of 10^{-8} M R6G were collected at 10 random positions and were shown in Fig. 5(d). It should be noted that all SERS spectra were obtained from three different samples under the same conditions. In the 10 spectra, the intensities of the characteristic peaks at 613 cm^{-1} and 1511 cm^{-1} were further illustrated in Figs. 5(e) and 5(f). The corresponding RSDs for the peaks at 613 cm^{-1} and 1511 cm^{-1} were calculated to be 5.20% and 8.00%, respectively. All the RSD values are less than 10%, indicating the excellent repeatability and uniformity of Ag/HLNAs for SERS applications.

3.3. *Electromagnetic enhancement mechanism*

To better understand the distribution of "hot spots" between the Ag NPs covered on flat substrate and HLNAs, the local electromagnetic field distributions of both the nanostructures were simulated using FDTD. Figures 6(a) and 6(b) displayed the 3D models based on simplified nanostructures of the Ag/flat Si and Ag/HLNAs, respectively. In two models, the diameters of the PS nanospheres and the Ag NPs were fixed at 300 nm and 30 nm, respectively. The gap between the Ag NPs was slightly varied from 3 nm to 8 nm according to the SEM. Then, a plane wave source with a wavelength of 532 nm was irradiated onto the nanostructures. In both nanostructures, the near-field coupling between neighboring Ag NPs caused enhanced local electromagnetic fields confined to narrow regions between NPs. As shown in Figs. 6(a-1) and 6(a-2), all "hot spots" existed simply between Ag NPs on the 2D plane. However, as compared to the 2D structure, more "hot spots" appeared between the Ag NPs around the PS nanospheres in HLNAs (Figs. 6(b-1) and 6(b-2)). The simulation results revealed that the rough PS sphere surface in Ag/HLNAs allowed the loading of more Ag NPs, and numerous 3D "hot spots" generated between them greatly enhanced the SERS effect.

3.4. *SERS performance of trace pesticide detection*

To further explore the substrate's possibilities for quantitative analysis of trace pesticides, the

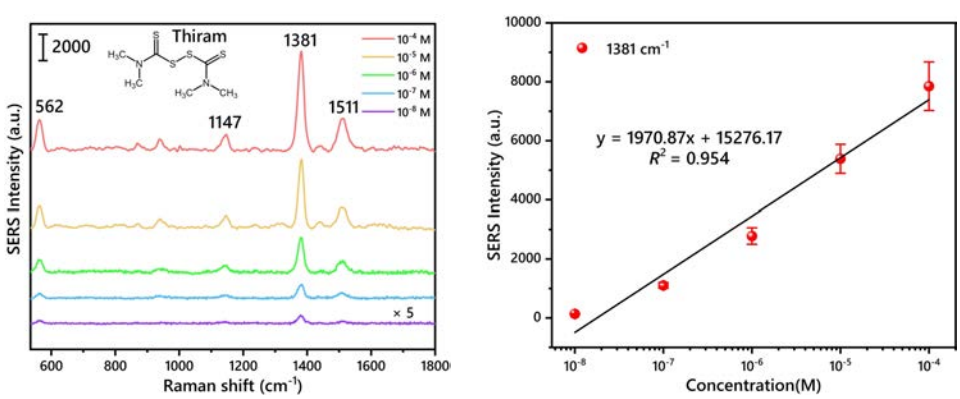

(a) (b)

Fig. 7. (a) Raman spectra of thiram with different concentrations obtained on the Ag/HLNAs. Inset shows the molecular structure of thiram. (b) Linear fitting curve between logarithmic thiram concentrations and their corresponding SERS intensity at 1381 cm^{-1} peak shift in (a).

Ag/HLNAs were applied to detect a dithiocarbamate compound (thiram). The Raman spectra of thiram in acetone solutions with varying concentrations are displayed in Fig. 7(a). A total of four characteristic peaks were distinguished at $562\,\mathrm{cm}^{-1}$, $1147\,\mathrm{cm}^{-1}$, $1381\,\mathrm{cm}^{-1}$, and $1511\,\mathrm{cm}^{-1}$ from the SERS spectra. The strongest peak at $1381\,\mathrm{cm}^{-1}$, which was attributed to C–N stretching as well as symmetric CH_3 deformation, was selected for the subsequent quantitative analysis. Therefore, even as the LOD of thiram reached up to 10^{-8} M, enhanced characteristic features at $1381\,\mathrm{cm}^{-1}$ were still observed. Moreover, the peak at $562\,\mathrm{cm}^{-1}$ was ascribed to S–S stretching.[32] As for the peak at $1147\,\mathrm{cm}^{-1}$, it was attributable to C–N stretching and CH_3 rocking. The peak located at $1511\,\mathrm{cm}^{-1}$ could be assigned to C–N stretching and CH_3 deformation.[32] Figure 7(b) further reveals a linear relationship between logarithmic thiram concentrations and their corresponding SERS intensity at $1381\,\mathrm{cm}^{-1}$. As the thiram concentration increased from 10^{-8} M to 10^{-4} M, the Raman intensity changed according to a good linear response with a large slope. The fitting equation was $y = 1970.87x + 15276.17$, with R^2 of 0.954. The above results demonstrate the prepared Ag/HLNAs based on improved self-assembly strategy with high sensitivity and uniformity possess enormous potential in SERS quantitative analysis of trace pesticides.

4. Conclusion

In summary, highly-ordered Ag/HLNAs were prepared by combining improved self-assembly, RIE, and e-beam evaporation, which provide a cost-effective and convenient approach for SERS measurements with high sensitivity and uniformity. It shows an excellent enhancement effects for R6G molecules with a LOD of 10^{-12} M and an EF of 2.79×10^7. It should be noted that an average RSD $< 10\%$ was obtained. In addition, thiram as one of the pesticides was detected up to a concentration of 10^{-8} M. Therefore, the Ag/HLNAs as effective SERS devices offer promising applications as in rapid detection of trace organic pollutants.

Conflicts of Interest

The authors declare that they have no known competing financial interests or personal relationships that could have appeared to influence the work reported in this paper.

Acknowledgments

This work was supported in part by the National Natural Science Foundation of China (61771467, 61774167, and 61801477), National Key Research and Development Program of China (2018YFC2001100), Youth Innovation Promotion Association, Chinese Academy of Sciences (2018153), and Key-Area Research and Development Program of Guangdong Province (2019B010117001).

References

1. S. Savary, A. Ficke, J.-N. Aubertot, C. Hollier, "Crop losses due to diseases and their implications for global food production losses and food security," *Food Security* **4**, 519–537 (2012).
2. H. Pu, Z. Huang, F. Xu, D. W. Sun, "Two-dimensional self-assembled Au–Ag core–shell nanorods nanoarray for sensitive detection of thiram in apple using surface-enhanced Raman spectroscopy," *Food Chem.* **343**, 128548 (2021).
3. B. Hu, D. W. Sun, H. Pu, Q. Wei, "A dynamically optical and highly stable pNIPAM @ Au NRs nanohybrid substrate for sensitive SERS detection of malachite green in fish fillet," *Talanta* **218**, 121188 (2020).
4. B. Hu, D. W. Sun, H. Pu, Q. Wei, "Rapid nondestructive detection of mixed pesticides residues on fruit surface using SERS combined with self-modeling mixture analysis method," *Talanta* **217**, 120998 (2020).
5. M. Fleischmann, P. J. Hendra, and A. J. McQuillan, "Raman spectra of pyridine adsorbed at a silver electrode," *Chem. Phys. Lett.* **26**(2), 163–166 (1974).
6. Z. Li, Z. Du, X. He, "Template-assisted electrodeposition of urchin-like Ag-nanoplate-assembled nanorod arrays and their structurally enhanced SERS performance," *J. Electrochem. Soc.* **164**(13), D895–D900 (2017).
7. J. Prinz, C. Heck, L. Ellerik, V. Merk, I. Bald, "DNA origami based Au–Ag–core–shell nanoparticle dimers with single-molecule SERS sensitivity," *Nanoscale* **8**(10), 5612–5620 (2016).
8. Q. Tao, S. Li, C. Ma, K. Liu, Q. Y. Zhang, "A highly sensitive and recyclable SERS substrate based on Ag-nanoparticle-decorated ZnO nanoflowers in ordered arrays," *Dalton Trans.* **44**(7), 3447–3453 (2015).

9. B. Zhou, J. Shen, P. Li, M. Ge, D. Lin, Y. Li, J. Lu, L. Yang, "Gold nanoparticle-decorated silver needle for surface-enhanced Raman spectroscopy screening of residual malachite green in aquaculture products," *ACS Appl. Nano Mater.* **2**(5), 2752–2757 (2019).
10. J. Krajczewski, A. Kudelski, "Shell-isolated nanoparticle-enhanced Raman spectroscopy," *Front. Chem.* **7**, 410 (2019).
11. A. K. Pal, S. Pagal, K. Prashanth, G. K. Chandra, S. Umapathy, D. B. Mohan, "Ag/ZnO/Au 3D hybrid structured reusable SERS substrate as highly sensitive platform for DNA detection," *Sens. Actuators B Chem.* **279**, 157–169 (2019).
12. X. Gao, J. Boryczka, P. Zheng, S. Kasani, F. Yang, E. B. Engler-Chiurazzi, J. W. Simpkins, J. G. Wigginton, N. Wu, "A "hot Spot"-Enhanced paper lateral flow assay for ultrasensitive detection of traumatic brain injury biomarker S-100β in blood plasma," *Biosens. Bioelectron.* **177**, 112967 (2021).
13. L. Ouyang, Y. Hu, L. Zhu, G. J. Cheng, J. Irudayaraj, "A reusable laser wrapped graphene-Ag array based SERS sensor for trace detection of genomic DNA methylation," *Biosens. Bioelectron.* **92**, 755–762 (2017).
14. L. Petti, R. Capasso, M. Rippa, M. Pannico, P. La Manna, G. Peluso, A. Calarco, E. Bobeico, P. Musto, "A plasmonic nanostructure fabricated by electron beam lithography as a sensitive and highly homogeneous SERS substrate for bio-sensing applications," *Vib. Spectrosc.* **82**, 22–30 (2016).
15. G. Barbillon, V. E. Sandana, C. Humbert, B. Belier, D. J. Rogers, F. H. Teherani, P. Bove, R. McClintock, M. Razeghi, "Study of Au coated ZnO nanoarrays for surface enhanced Raman scattering chemical sensing," *J. Mater. Chem. C.* **5**(14), 3528–3535 (2017).
16. M. Fan, G. F. Andrade, A. G. Brolo, "A review on the fabrication of substrates for surface enhanced Raman spectroscopy and their applications in analytical chemistry," *Anal. Chim. Acta.* **693**(1–2), 7–25 (2011).
17. L. Qin, S. Zou, C. Xue, A. Atkinson, G. C. Schatz, C. A. Mirkin, "Designing, fabricating, and imaging Raman hot spots," *Proc. Natl. Acad. Sci. U. S. A.* **103**(36), 13300–13303 (2006).
18. H. Im, K. C. Bantz, S. H. Lee, T. W. Johnson, C. L. Haynes, S. H. Oh, "Self-assembled plasmonic nanoring cavity arrays for SERS and LSPR biosensing," *Adv. Mater.* **25**(19), 2678–2685 (2013).
19. H. Mao, W. Wu, D. She, G. Sun, P. Lv, J. Xu, "Microfluidic surface-enhanced Raman scattering sensors based on nanopillar forests realized by an oxygen-plasma-stripping-of-photoresist technique," *Small* **10**(1), 127–134 (2014).
20. J. Huang, Z. He, Y. Liu, L. Liu, X. He, T. Wang, Y. Yi, C. Xie, K. Du, "Large surface-enhanced Raman scattering from nanoporous gold film over nanosphere," *Appl. Surf. Sci.* **478**, 793–801 (2019).
21. A. E. Cetin, C. Yilmaz, B. C. Galarreta, G. Yilmaz, H. Altug, A. Busnaina, "Fabrication of sub-10-nm plasmonic gaps for ultra-sensitive Raman spectroscopy," *Plasmonics* **15**(4), 1165–1171 (2020).
22. Z. Huang, G. Meng, Q. Huang, Y. Yang, C. Zhu, C. Tang, "Improved SERS performance from Au nanopillar arrays by abridging the pillar tip spacing by Ag sputtering," *Adv. Mater.* **22**(37), 4136–4139 (2010).
23. G. Liu, X. Li, W. Wang, F. Zhou, G. Duan, Y. Li, Z. Xu, W. Cai, "Gold binary-structured arrays based on monolayer colloidal crystals and their optical properties," *Small* **10**(12), 2374–2381 (2014).
24. W. Yue, T. Gong, X. Long, V. Kravets, P. Gao, M. Pu, C. Wang, "Sensitive and reproducible surface-enhanced Raman spectroscopy (SERS) with arrays of dimer-nanopillars," *Sens. Actuators B Chem.* **322**, 128563 (2020).
25. S. Bai, D. Serien, A. Hu, K. Sugioka, "3D microfluidic surface-enhanced Raman spectroscopy (SERS) chips fabricated by all-femtosecond-laser-processing for real-time sensing of toxic substances," *Adv. Funct. Mater.* **28**(23), 1706262 (2018).
26. K. Sivashanmugan, J. D. Liao, J. W. You, C. L. Wu, "Focused-ion-beam-fabricated Au/Ag multilayered nanorod array as SERS-active substrate for virus strain detection," *Sens. Actuators B Chem.* **181**, 361–367 (2013).
27. S. Li, N. Zhang, N. Zhang, D. Lin, X. Hu, X. Yang, "Three-dimensional ordered Ag/ZnO/Si hierarchical nanoflower arrays for spatially uniform and ultrasensitive SERS detection," *Sens. Actuators B: Chem.* **321**, 128519 (2020).
28. X. Li, Y. Zhang, M. Li, Y. Zhao, L. Zhang, C. Huang, "Convex-meniscus-assisted self-assembly at the air/water interface to prepare a wafer-scale colloidal monolayer without overlap," *Langmuir* **37**(1), 249–256 (2021).
29. H. Zhang, D. Liu, L. Hang, X. Li, G. Liu, W. Cai, Y. Li, "Effective SERS-active substrates composed of hierarchical micro/nanostructured arrays based on reactive ion etching and colloidal masks," *Nanotechnology* **27**(39), 395304 (2016).
30. Z. Li, G. Meng, Q. Huang, X. Hu, X. He, H. Tang, Z. Wang, F. Li, "Ag nanoparticle-grafted PAN-nanohump array films with 3D high-density hot spots as flexible and reliable SERS substrates," *Small* **11**(40), 5452–5459 (2015).
31. R. Li, B. Gui, H. Mao, Y. Yang, D. Chen, J. Xiong, "Self-concentrated SERS-active droplet sensor with three-dimensional hot spots for highly sensitive

molecular detection in complex liquid environments," *ACS Sens.* **5**(11), 3420–3431 (2020).

32. J. Chen, Y. Huang, P. Kannan, L. Zhang, Z. Lin, J. Zhang, T. Chen, L. Guo, "Flexible and adhesive surface enhance Raman scattering active tape for rapid detection of pesticide residues in fruits and vegetables," *Anal. Chem.* **88**(4), 2149–2155 (2016).
33. X. Zheng, Y. Chen, Y. Chen, N. Bi, H. Qi, M. Qin, D. Song, H. Zhang, Y. Tian, "High performance Au/Ag core/shell bipyramids for determination of thiram based on surface-enhanced Raman scattering," *J. Raman Spectrosc.* **43**(10), 1374–1380 (2012).